Journal of Thermal Analysis and Calorimetry, Vol. 59 (2000) 683–697

Dedicated to Prof. Edith A. Turi in recognition of her leadership in education

HEAT CAPACITIES AND THERMAL PROPERTIES OF A HOMOGENEOUS ETHYLENE-1-OCTENE COPOLYMER BY ADIABATIC CALORIMETRY

P. J. van Ekeren[1]*, L. D. Ionescu*[1]*, V. B. F. Mathot*[2] *and J. C. van Miltenburg*[1]

[1]Chemical Thermodynamics Group, Debye Institute, Utrecht University, Padualaan 8 3584 CH Utrecht
[2]DSM Research, P.O. Box 18, 6160 MD Geleen, The Netherlands

Abstract

Specific heat capacities of a homogeneous ethylene-1-octene copolymer were measured by adiabatic calorimetry in the temperature range from 5 to 400 K (stepwise heating at averaged rates of approximately 1 to 34 K h^{-1}, after cooling at rates in the range from 8 K h^{-1} to 4 K min^{-1}). The glass transition takes place from roughly 205 to 225 K and is centred around approximately 215 K. At the latter temperature, also the temperature drifts during the stabilisation periods are at maximum. Clearly, with devitrification above 215 K also melting sets in. Using two sets of reference data (one for branched and linear polyethylenes, BPE, and the other for strictly linear polyethylene, LPE) for completely crystalline and for completely amorphous material, the crystallinity of the polymer was calculated as a function of temperature, within the two-phase model. In heating, the crystallinity decreased from 0.254 to zero in the temperature range from 220 to 360 K, confirming earlier DSC heat capacity measurements. During the stabilisation periods, below 325 K, negative drifts were observed, related to endothermic effects caused by melting. However, in the temperature range from 325 K up to the end melting temperature, 360 K, positive drifts were measured, reflecting exothermic effects. These are attributed to recrystallisation phenomena. The occurrence and amount of recrystallisation depend on the thermal history of the sample: slower cooling and a longer time spent at a temperature of annealing clearly diminish recrystallisation.

Keywords: adiabatic calorimetry, crystallinity, ethylene-1-octene copolymer, heat capacity, recrystallisation, relaxation

Introduction

The thermal behaviour of polymers is nowadays widely investigated using differential scanning calorimetry [1]. To support these investigations with very accurate heat capacity data, it was decided to measure the heat capacity of some ethylene-1-alkene copolymers over very large temperature ranges using adiabatic calorimetry. First results, obtained for a heterogeneous ethylene-1-octene very low density polyethylene (VLDPE) with a comonomer content of 6.2 mole% and a density of 902 kg m^{-3}, were published in a previous paper [2]. In this paper the results for a homogeneous ethyl-

1418–2874/2000/ $ 5.00

Akadémiai Kiadó, Budapest
Kluwer Academic Publishers, Dordrecht

ene-1-octene copolymer with a comonomer content of 13.6 mole% and a density of 870 kg m^{-3} will be presented.

Experimental

The sample

The sample, which was supplied by DSM and indicated as EO M, is a homogeneous ethylene-1-octene copolymer. For the production of this material use was made of metallocene based catalysis [3, 4]. The density of the material (at 298 K, after compression moulding) is 870 kg m^{-3}. The molar percentage of 1-octene is 13.6% (i.e. the mass percentage of 1-octene is 38.7%). The molar mass distribution by SEC of the sample is indicated by M_n=42 kg mol^{-1}, M_w=91 kg mol^{-1} and M_z=150 kg mol^{-1}.

The adiabatic calorimeter

The measurements were performed using one of our home-built adiabatic calorimeters. The calorimeter, the design of which recently has been improved [5], was described previously [6]. The thermometer is a 27 Ω rhodium-iron resistance, which has been calibrated by Oxford Instruments at 33 points between 1.5 and 300 K. The calibration was extended to 430 K using the melting temperatures of naphthalene and indium. Conversion to the ITS-90 scale is based on the article of Preston-Thomas [7].

After filling, the calorimeter vessel is evacuated. Helium gas is admitted to the vessel until the pressure is about 1000 Pa. Measurements are made in the intermittent mode. This implies that stabilisation periods are followed by input periods under automatic control. During each stabilisation period, the temperature is recorded as a function of time. Between two stabilisation periods, an input period is used to raise the temperature of the sample. The amount of heat added to the calorimeter vessel is measured very accurately. The temperature increase, which is caused by this heat input, follows from extrapolation of the temperature-time curves of both stabilisation periods. These data allow for the accurate calculation of the heat capacity. The heat capacity of the empty calorimeter vessel must be subtracted to obtain the heat capacity of the sample. In the transition regions thermal equilibrium is not reached within a practical time limit because of relaxation processes. Therefore in these regions another method was applied. Using the known heat transfer to the surroundings (from an empty vessel experiment) together with the applied electrical energy, the enthalpy increment between (the midpoints of) two successive stabilisation periods is calculated, resulting in the actual enthalpy path of the vessel and its content.

Because heat exchange with the surroundings is very small (due to the adiabatic construction), temperature drifts observed in the stabilisation periods may be used to investigate relaxation processes.

According to measurements of standard materials, the inaccuracy is approximately 0.2% of the absolute heat capacity.

Table 1 Overview of the series of measurements performed on the EO M sample. For each measurement series the temperature range in which measurements were performed is given together with the duration of the stabilisation and input periods and the averaged heating rates <β>

Series nr.	T_1/K	T_2/K	t(stab.)/s	t(input)/s	<β> / Kh^{-1}
1	297	380	600	808	5
2	100	277	600	808	7
3	278	400	600	808	5
4	5	24	100	100	34
5	5	33	200	100	26
6	17	33	200	204	1
7	34	100	400	508	10
8	100	300	2000	808	3.5

The measurements

The calorimeter vessel was filled with an amount of 5.6735 g of the polymer. Eight series of measurements were performed with this sample in the temperature range from 5 to 400 K. An overview of the performed measurements (temperature ranges, duration of stabilisation and input periods and averaged heating rates) is given in Table 1. Series 1 was started at 297 K, after long time storage (some years) at room temperature, and ended at 380 K. The sample was kept at this temperature for several hours. Controlled cooling of the sample in the adiabatic calorimeter is not possible (i.e. heat capacity measurements during cooling are also not possible). After series 1 the sample was cooled by switching off the temperature control of the shields. This resulted in an average cooling rate of approximately 8 K h^{-1} in the range where crystallisation takes place. To have an impression of the thermal history of the sample, the temperature of the calorimeter vessel was recorded during cooling from 380 to 170 K. This cooling curve is plotted in Fig. 1. The cooling continued down to 100 K, at which temperature series 2 was started, ending at 277 K. After a waiting

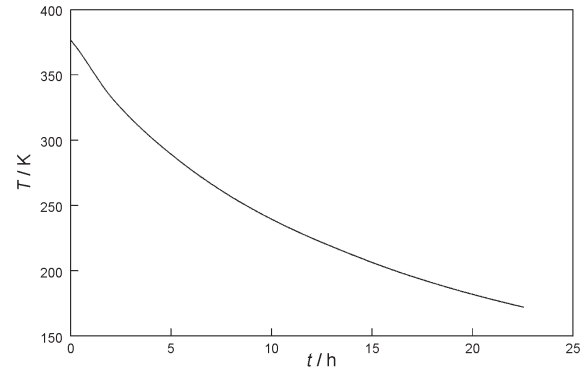

Fig. 1 Cooling curve, recorded after measurement series 1

time of some hours, series 3 was started, ending at 400 K. Then, after a waiting time of several hours, the sample was cooled down to 4 K. No cooling curve was recorded, but for the cooling from 380 to 170 K the thermal history should be similar to that observed during cooling after series 1 (Fig. 1). Below 170 K the sample was cooled faster (cooling rates up 4 K min^{-1}) by breaking the vacuum and admitting helium gas. After series 4 and 5 the sample was cooled to 4 and 17 K, respectively. After series 6 and 7 the sample was not cooled. Between the end of series 6 and the start of series 7 the sample was kept at 33 K for about 0.5 h; between the end of series 7 and the start of series 8 the sample was kept at 100 K for approximately 12 h.

Results and discussion

Specific heat capacity

The specific heat capacities that were evaluated from the measurements are given in Table 2.

Table 2 Measured specific heat capacity as a function of temperature

T/K	c_p/ J K^{-1} g^{-1}	T/K	c_p/ J K^{-1} g^{-1}	T/K	c_p/ J K^{-1} g^{-1}	T/K	c_p/ J K^{-1} g^{-1}
Series 1		331.59	3.226	372.37	2.409	139.72	0.923
297.50	2.449	333.56	3.230	374.37	2.418	142.64	0.939
298.21	2.484	335.53	3.224	376.37	2.426	145.56	0.955
299.55	2.484	337.51	3.205	378.38	2.435	148.49	0.971
301.51	2.549	339.50	3.169	380.38	2.436	151.41	0.986
303.45	2.620	341.51	3.110	**Series 2**		154.34	1.002
305.36	2.699	343.55	3.022	100.91	0.707	157.27	1.018
307.25	2.793	345.61	2.911	102.51	0.717	160.20	1.034
309.12	2.919	347.70	2.796	104.77	0.729	163.13	1.049
310.94	3.120	349.82	2.687	107.69	0.743	166.06	1.066
312.70	3.398	351.94	2.587	110.59	0.762	168.99	1.083
314.40	3.535	354.05	2.507	113.49	0.778	171.92	1.101
316.15	3.466	356.16	2.452	116.39	0.794	174.85	1.117
317.97	3.346	358.23	2.419	119.30	0.810	177.78	1.136
319.86	3.249	360.28	2.401	122.21	0.827	180.70	1.154
321.80	3.194	362.32	2.393	125.13	0.843	183.63	1.173
323.75	3.178	364.34	2.390	128.04	0.859	186.55	1.191
325.71	3.184	366.35	2.392	130.96	0.875	189.47	1.211
327.67	3.200	368.36	2.397	133.88	0.891	192.39	1.232
329.63	3.216	370.36	2.402	136.80	0.907	195.30	1.254

T/K	c_p/ J K^{-1} g^{-1}	T/K	c_p/ J K^{-1} g^{-1}	T/K	c_p/ J K^{-1} g^{-1}	T/K	c_p/ J K^{-1} g^{-1}
198.21	1.278	284.73	2.664	356.39	2.418	**Series 5**	
201.11	1.305	286.67	2.678	358.43	2.392	5.46	0.009
204.00	1.336	288.61	2.696	360.45	2.386	6.46	0.009
206.88	1.375	290.56	2.715	362.45	2.387	8.03	0.015
209.74	1.428	292.51	2.734	364.44	2.392	9.87	0.024
212.56	1.501	294.46	2.753	366.42	2.398	11.60	0.033
215.34	1.589	296.41	2.772	368.40	2.405	13.55	0.047
218.09	1.671	298.37	2.790	370.38	2.413	15.65	0.060
220.84	1.739	300.33	2.807	372.37	2.423	17.84	0.078
223.61	1.796	302.29	2.824	374.35	2.432	20.14	0.095
226.43	1.849	304.26	2.839	376.33	2.439	22.55	0.114
229.24	1.897	306.22	2.857	378.31	2.437	25.03	0.134
232.02	1.939	308.19	2.873	380.30	2.439	27.59	0.148
234.75	1.978	310.15	2.889	382.29	2.458	30.25	0.162
237.46	2.014	312.12	2.906	384.27	2.455	32.93	0.178
240.13	2.049	314.09	2.924	386.25	2.452	**Series 6**	
242.78	2.083	316.06	2.944	388.24	2.458	17.16	0.072
245.40	2.115	318.03	2.965	390.22	2.465	17.44	0.074
247.99	2.147	320.00	2.989	392.20	2.469	19.24	0.087
250.56	2.179	321.96	3.013	394.18	2.473	22.14	0.111
253.10	2.210	323.93	3.036	396.17	2.478	24.59	0.130
255.62	2.237	325.90	3.053	398.15	2.484	27.16	0.149
258.12	2.269	327.87	3.066	400.13	2.488	29.87	0.164
260.60	2.300	329.84	3.071	**Series 4**		32.63	0.185
263.06	2.331	331.83	3.069	5.06	0.005	**Series 7**	
265.50	2.345	333.82	3.064	6.19	0.008	34.29	0.200
267.92	2.391	335.82	3.054	7.47	0.013	34.81	0.206
270.31	2.422	337.83	3.037	9.11	0.020	36.45	0.237
272.68	2.452	339.85	3.007	10.80	0.029	39.08	0.258
275.03	2.483	341.88	2.960	12.65	0.040	41.55	0.280
277.37	2.513	343.92	2.895	14.66	0.053	44.00	0.302
Series 3		345.98	2.817	16.80	0.067	46.48	0.323
278.87	2.482	348.06	2.736	19.04	0.082	48.99	0.345
279.56	2.522	350.15	2.651	21.36	0.100	51.52	0.367
280.88	2.576	352.23	2.562	23.71	0.122	54.07	0.388
282.81	2.647	354.32	2.477			56.64	0.409

T/K	c_p/ J K^{-1} g^{-1}	T/K	c_p/ J K^{-1} g^{-1}	T/K	c_p/ J K^{-1} g^{-1}	T/K	c_p/ J K^{-1} g^{-1}
59.23	0.429	118.57	0.805	188.69	1.203	255.48	2.205
61.83	0.449	121.48	0.821	191.62	1.223	257.98	2.236
64.45	0.469	124.39	0.838	194.56	1.244	260.46	2.270
67.08	0.488	127.30	0.856	197.49	1.267	262.92	2.301
69.72	0.506	130.22	0.873	200.42	1.292	265.36	2.331
72.37	0.525	133.14	0.889	203.35	1.321	267.77	2.362
75.03	0.542	136.06	0.904	206.26	1.358	270.16	2.393
77.70	0.559	138.98	0.921	209.17	1.408	272.53	2.422
80.39	0.576	141.90	0.937	212.04	1.476	274.89	2.451
83.07	0.593	144.82	0.954	214.88	1.561	277.22	2.482
85.77	0.609	147.74	0.969	217.70	1.642	279.53	2.509
88.46	0.626	150.66	0.986	220.52	1.712	281.83	2.538
91.16	0.642	153.58	1.001	223.36	1.774	284.11	2.565
93.85	0.658	156.49	1.017	226.21	1.827	286.37	2.590
96.54	0.673	159.41	1.033	229.03	1.873	288.62	2.615
99.23	0.689	162.33	1.047	231.81	1.914	290.85	2.638
Series 8		165.25	1.066	234.56	1.952	293.07	2.661
101.29	0.719	168.17	1.081	237.27	1.988	295.27	2.683
102.10	0.706	171.10	1.098	239.95	2.022	297.46	2.702
104.00	0.721	174.03	1.115	242.60	2.055	299.65	2.720
106.94	0.736	176.95	1.132	245.23	2.086		
109.87	0.735	179.89	1.149	247.83	2.117		
112.78	0.768	182.82	1.167	250.40	2.149		
115.68	0.788	185.75	1.185	252.95	2.179		

The heat capacities that were measured in the series 1, 2 and 3 are plotted as a function of temperature in Fig. 2. For temperatures below about 350 K the results of series 1 deviate considerably from those of series 3. This is caused by the different thermal history of the sample for these measurements. Series 1 was performed on the sample as received, thus after a long storage time (years) at room temperature. During this annealing the sample had obviously relaxed to a more stable state. The small discontinuity observed around 280 K (the first measurements of series 3) is also caused by annealing: between the end of series 2 and the start of series 3 the temperature was kept constant for some hours. At temperatures above 360 K, where the sample appears to be completely molten, the results of series 1 and series 3 are in good agreement. The results are also in good agreement with (estimated) specific heat capacity data of (metastable) liquid LPE as given by Wunderlich *et al.* [8] (and adopted by Mathot [9]):

$$c_p(\text{LPE, liq, } T)/(\text{J K}^{-1}\ \text{g}^{-1}) = 1.426 + 2.401\cdot10^{-3}T/\text{K} + 7.065\cdot10^{-7}(T/\text{K})^2 \qquad (1)$$

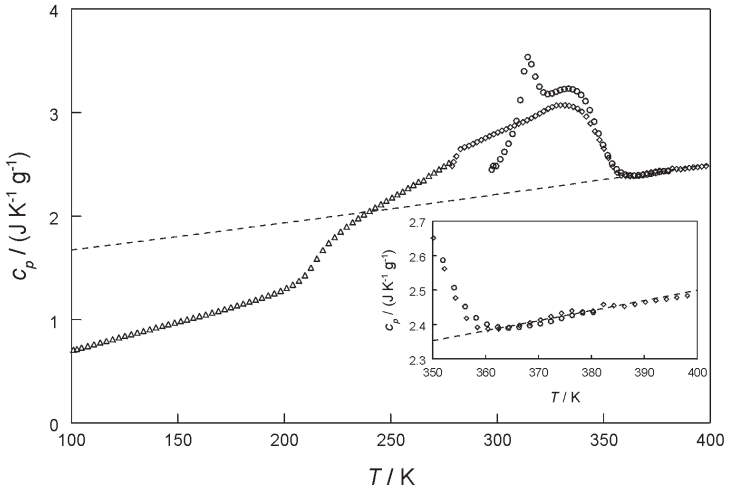

Fig. 2 Specific heat capacity of EO M as a function of temperature. o – series 1 (sample as received); Δ – series 2; ✧ – series 3. --- – specific heat capacity of (metastable) liquid linear polyethylene (LPE) according to Eq. (1). Insert: magnification for the liquid region (350≤T/K≤400 K)

For very low density polyethylene (VLDPE) a remarkable progressive increase of the specific heat capacity of the polymer in its liquid state was observed by adiabatic calorimetry between subsequent series of measurements [2]. This phenomenon was not observed for this EO M sample.

Temperature range 5 to 125 K

The results obtained for low temperatures (T<125 K) are plotted in Fig. 3. Also plotted in this figure are reference data for completely amorphous and for completely crystalline polyethylene (BPE), as given in the ATHAS data bank [10] (Fig. 3a), and data presented by Mathot [9] for completely amorphous and for completely crystalline LPE (Fig. 3b). The results of series 4, 5 and 6, obtained at temperatures below 35 K, are in excellent agreement with each other. It appears that a small anomaly was observed in the temperature range 25 to 35 K; its cause is not clear at the moment.

Besides the temperature range in which the small anomaly was observed (between 25 and 35 K) our heat capacity data for EO M are very close to the heat capacity of completely amorphous polyethylene (BPE) according to the ATHAS data bank [10] (Fig. 3a). Our data are slightly below the heat capacity of completely amorphous LPE as given by Mathot [9] up to about 65 K (Fig. 3b). Above about 65 K, however, our heat capacity data are above the heat capacity of completely amorphous LPE.

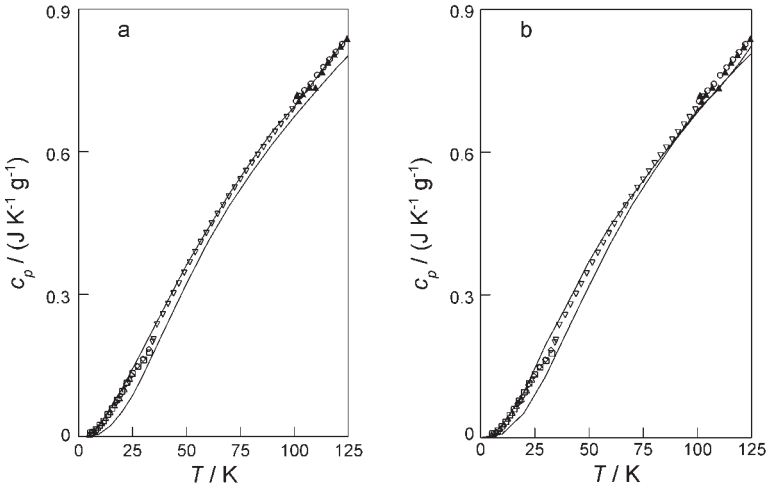

Fig. 3 Low temperature specific heat capacity data for EO M. o – series 2; Δ – series 4; □ – series 5; ◇ – series 6; ▽ – series 7; ▲ – series 8. In Fig. 3 (a) the solid lines represent specific heat capacity data for completely crystalline and completely amorphous polyethylene (BPE) according to the ATHAS data bank [10], in Fig. 3 (b) the solid lines represent the data for completely amorphous and completely crystalline LPE according to Mathot [9]. Specific heat capacities for the completely amorphous phase are larger than those for the completely crystalline phase

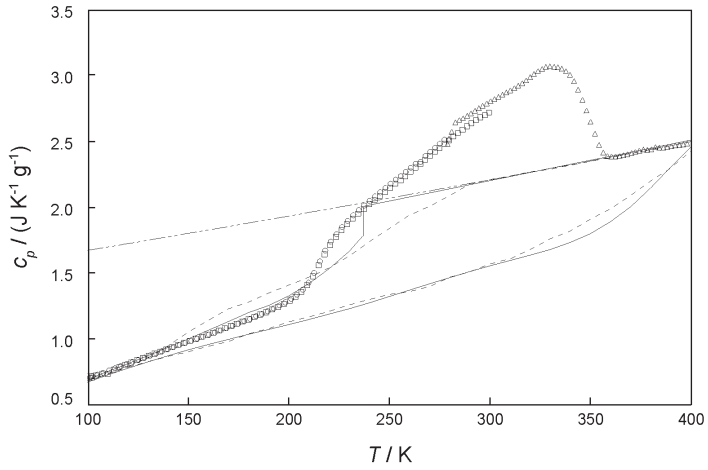

Fig. 4 Specific heat capacity data for EO M in the glass transition and melting region. o – series 2; Δ – series 3; □ – series 8. The solid and the dashed lines represent reference data for BPE according to the ATHAS data bank [10] and for LPE according to Mathot [9], respectively. Reference data are given for completely amorphous and for completely crystalline phases. The dash-dotted line representscording to the specific heat capacity of (metastable) liquid LPE ac Eq. (1)

Temperature range 100 to 400 K

Data obtained in the temperature range from 100 to 400 K (i.e. the range where devitrification and melting take place; measurements from series 1 are omitted in this figure) are plotted in Fig. 4, together with the reference data for BPE and for LPE.

In the temperature range from approximately 150 to 200 K the measured specific heat capacity of EO M is slightly smaller than the specific heat capacity of completely amorphous BPE and considerably larger than the specific heat capacity of completely crystalline BPE, roughly confirming a crystallinity of EO M of approximately 0.25, as calculated from the melting region (see further).

As is seen in Fig. 4, the amorphous phase of the EO M sample devitrifies in the temperature range from roughly 205 K to 225 K and is centred around approximately 215 K (see also the discussion with respect to the minima in the temperature drifts at the same temperature in Fig. 7). According to the ATHAS data bank, the glass transition temperature for completely amorphous BPE is 237 K which is shown as a sharp jump of the heat capacity in the figure. Our EO M sample clearly devitrifies at a lower temperature. For completely amorphous LPE in heating a gradually increasing heat capacity in the temperature range from 120 to 290 K was found, which could be interpreted as a reflection of a continuous devitrification process; see [9] for a discussion and for other possibilities.

Above about 125 K, the c_p data for EO M are in between the c_{pa} and c_{pc} data for LPE, as expected. Because homogeneous copolymers like EO M, but also heterogeneous ones like linear low density polyethylene (LLDPE) and very low density polyethylene (VLDPE), clearly show glass transitions in relatively narrow temperature ranges, the reference heat capacities for the completely amorphous state of LPE are clearly not usable below 290 K, because of their gradual change over a wide temperature range (120–290 K). The data for BPE also poses a problem because of the higher glass transition temperature. For that reason, in previous publications we used also below 290 K – down to the glass transition temperature measured – the continuation of Eq. (1) as $c_{pa}(T)$.

From Fig. 4 it is likely that melting of the crystalline phase of the sample starts in this devitrification range too. This is in accordance with previous results [11, 12] for this sample, where melting gave rise to excess heat capacity above approximately 230 K during heating at 20 K min^{-1} after cooling at the same rate.

Crystallinity

The enthalpy-based mass fraction crystallinity of EO M, as defined within the two-phase model, may be calculated using the following equation [13]:

$$w^{c}(T)=\frac{h_a(T)-h(T)}{h_a(T)-h_c(T)} \tag{2}$$

where $h_a(T)$ is the specific enthalpy of the completely amorphous phase, $h_c(T)$ the specific enthalpy of the completely crystalline phase and $h(T)$ the specific enthalpy of

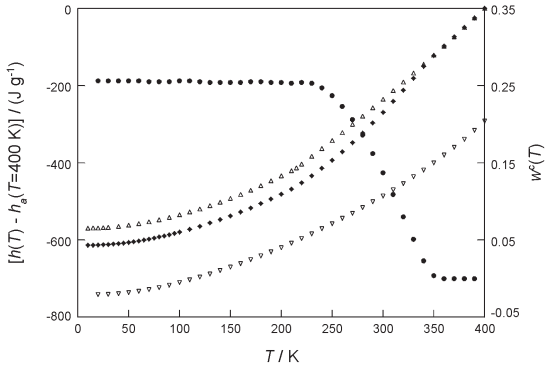

Fig. 5 Specific enthalpy of the semi-crystalline EO M sample (◆), together with the specific enthalpy of the crystalline phase (∇) and of the amorphous phase (Δ). The enthalpy-based mass crystallinity (scaling given on the right vertical axis) of the EO M sample is also plotted (●)

the semi-crystalline sample. Because the enthalpy function does not have a natural zero-point (e.g. [14]), a common reference point has to be defined. Here the specific enthalpy of EO M at a temperature of 400 K, where EO M appears to be completely molten and which is the highest temperature of our measurements, is taken as the reference point for the enthalpy function. Because EO M is completely molten at T=400 K, it may be stated that $h_a(T=400\,\mathrm{K})=h(T=400\,\mathrm{K})$.

The specific enthalpy as a function of temperature may be found by integrating the specific heat capacity:

$$h(T=\Theta)-h(T=400\,\mathrm{K})=\int_{T=400\,\mathrm{K}}^{T=\Theta} c_p(T)\,\mathrm{d}T \tag{3}$$

It is assumed here that the specific enthalpy of the crystalline phase is equal to the specific enthalpy of completely crystalline LPE as given by Mathot [9], corrected for the difference in reference point. The specific enthalpy of the amorphous phase is calculated using Eq. (3) by assuming that:

- the glass transition temperature is T_g=215 K;
- the specific heat capacity of the amorphous phase above the glass transition temperature is equal to the specific heat capacity of (super-cooled) liquid LPE (given by Eq. (1));
- the specific heat capacity of the amorphous phase below the glass transition temperature is taken to be equal to the specific heat capacity of amorphous BPE in its glassy state as given by the ATHAS data bank [10].

The specific enthalpies thus found are plotted in Fig. 5, together with the enthalpy-based mass crystallinity calculated using Eq. (2). In the temperature range from 230 to 360 K the crystallinity gradually decreases from 0.254 to zero, caused by melting of the crystalline phase. This is in good agreement with the crystallinity calculated by Mathot *et al.* [11] using heat capacity curves measured by DSC on heating.

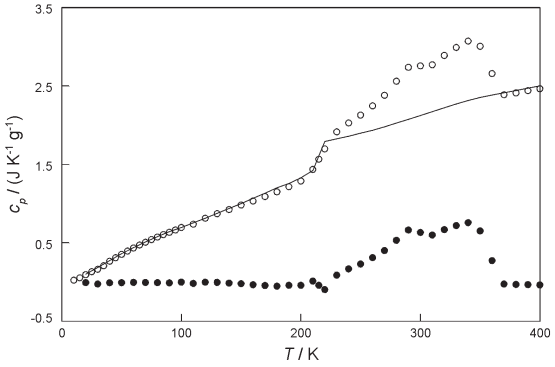

Fig. 6 Experimental specific heat capacity of EO M (o) together with the specific base line heat capacity (solid line) and the specific excess heat capacity (•)

They found crystallinities of 0.24 at 227 K, 0.19 at 273 K and 0.15 at 293 K whereas our values at the same temperatures are 0.25, 0.20 and 0.15, respectively. The values do not deviate significantly, surprisingly, though Mathot *et al.* used a cooling rate of 20 K min^{-1} whereas our cooling rates were much lower.

Base-line and excess heat capacities

Using the evaluated crystallinity of EO M as a function of temperature, the so-called specific base line heat capacity [13] of EO M may be calculated using the following equation:

$$c_{p\mathrm{b}}(T)=w^{\mathrm{c}}(T)c_{p\mathrm{c}}(T)+[1-w^{\mathrm{c}}(T)]c_{p\mathrm{a}}(T)$$

The specific excess heat capacity may be calculated by subtracting the specific base line heat capacity from the experimental specific heat capacity:

$$c_{p\mathrm{e}}(T)=c_p(T)-c_{p\mathrm{b}}(T)$$

These important functions are plotted in Fig. 6. The specific excess heat capacity function obtained resembles the function obtained by Mathot *et al.* [11] using DSC on heating at 20 K min^{-1} after cooling at the same rate.

Relations with molecular structure and morphology

The shape of the heating curve is influenced by thermal history as can be seen in Fig. 2. Cooling rate and heating rate, storage or annealing all affect the specific way of melting. Also, depending on these parameters, recrystallisation can occur, see further. In general, the whole sample history plays a role, including additional parameters like possible orientation as a result of processing, nucleation by additives as added after polymerisation, etc. Even the way of polymerisation can be crucial because the specific chain topology can be unique. This is also expected if crystalli-

sation takes place during polymerisation, leading to possible non-reversible topology and morphology.

However, the molecular structure is also a dominant parameter. The chain lengths present, reflected by the molar mass distribution, influence crystallisation and melting [15]. For copolymers, the amount and distribution of comonomer units along the chains have a major impact, as can be seen from the remarkable differences between homogeneous and heterogeneous copolymers as produced by catalysts having one active site or at least two active sites [15]. These differences on a molecular scale proceed via a different crystallisation behaviour and resulting different morphologies to different end-properties. Of use is DSC, because it is able to measure the differences in crystallisation and melting behaviour, giving the opportunity – though only after proper 'calibration' – to interpret the thermal behaviour into molecular characteristics.

Homogeneous copolymers, like EO M, are defined as consisting of molecules polymerised using a catalyst with one active site, producing copolymerized chains with defined statistics of monomer and comonomer inclusions, irrespective of chain length. The statistics of comonomer inclusion leads to single-peaked distributions of the 1-octene units and of the ethylene units according to their sequence lengths. For crystallisation this distribution of the crystallisable ethylene sequence lengths is of utmost importance, because it rules the crystallisability of the copolymer as such: 1-octenes cannot be incorporated in the crystallites because of their bulky character. Of course, the other parameters mentioned influence whether or not crystallisability is matched by actual crystallisation.

Though one would expect a simple relation between the ethylene sequence length distribution (ESLD) and the resulting crystallite dimension distribution, this is in practice not the case. Copolymers, like homopolymers, have to crystallise through a nucleation step, which is quite difficult for these because of their long chain character and concomitant diffusion problems. Also the connectivity of sequences of different lengths within the same chain poses a problem in the process of matching sequences of the same length in a crystallite. For such reasons, crystallisation takes place at supercoolings, which can be appreciable. Thus, because of the kinetic restrictions as a result of the macromolecular character, copolymers do not crystallise in equilibrium. For instance, most ethylene sequences will not be present in extended form in the crystallites, because the kinetic restrictions for nucleation will lead to nuclei with dimensions that are smaller than the sequence lengths available. By that, and also in order to avoid crowding at the crystallite surface, the longest ethylene sequences will have to fold to match the dimension of a stable nucleus. This will lead to a non-trivial relation between the ESLD and the crystallite dimension distribution and also to a potentially unstable situation, leading to possible effects during annealing like reorganisation or even recrystallisation. Melting will reflect the actual crystallite dimension distribution at the specific temperature. For that reason the term 'calibration' was used to describe the non-trivial linkage of the constituent parts of the chain: ESLD⇔crystallisation temperature distribution⇔crystallite dimension distribution/morphology⇔melting temperature distribution.

Returning to Figs 2 and 4, it will be clear that the broad melting range of EO M is caused by the broad ESLD. It is to be expected, based on an evaluation of the polymerisation kinetics on the basis of ^{13}C-NMR data [15], that the maximum of the distribution of the ethylene sequence lengths will be approximately 7, while sequences up to approximately 50 will be present. Most 1-octene units will occur isolated or in pairs. In line with the forgoing, the morphology of EO M is not of a single type but shows a granular base morphology (as formed by the shorter sequences) with additional lamellar structures as formed by the longer sequences [12].

Heterogeneous copolymers, having at least two active sites and by that having at least a superposition of two ESLDs, even show much wider crystallisation and melting temperature distributions. Also the morphology reflects this, by presence of a wealth of different crystallite dimensions [15].

Temperature drifts during stabilisation

The temperature drifts of the sample and calorimeter vessel, which were recorded in the stabilisation periods (in fact evaluated from a linear fit of the temperature *vs*. time curve in the second half of the stabilisation periods) of the measurement series 1, 2, 3 and 8, are plotted in Fig. 7. Usually, in a transition region characterised by an endothermic heat effect, negative drifts are observed, reflecting melting. During series 1 and 3, however, at higher temperatures (above approximately 340 and 325 K for series 1 and 3, respectively) also positive temperature drifts were detected: up to about 15 μK s^{-1} (Fig. 7). This implies that in this part of the melting region a relaxation process occurs in the stabilisation periods, which must be interpreted as recrystallisation. The negative drifts for series 1 (up to –150 μK s^{-1}) and 3 with local minima at approximately 315 and 280 K, respectively, are related to the temperature at which annealing took place (room temperature and 277 K, respectively) and to the time it took (some years for series 1 and some hours for series 3). The temperature drifts observed during the stabilisation periods of series 8 are somewhat smaller because the stabilisation periods during series 8 lasted longer (2000 s for series 8 in stead of 600 s for se-

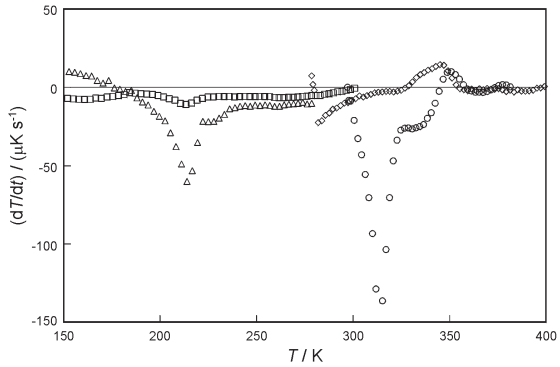

Fig. 7 Temperature drifts observed during the stabilisation periods. o – series 1 (sample as received); Δ – series 2; ✧ – series 3; □ – series 8

ries 1, 2 and 3). The negative drifts at low temperatures, with minima at 215 K, are caused by the devitrification process.

Interesting is the fact that also in case of very low density polyethylene (VLDPE), in heating after cooling at approximately 4 K min^{-1}, below 320 K negative drifts (melting phenomena) were measured while at all temperatures above 320 K only positive drifts (recrystallisation phenomena) were measured, all the way to the end of melting. For very slow cooling, 1 K h^{-1}, the exothermic effect was much smaller and the temperature drift became negative (only melting) just before the end of the melting range [2].

Obviously, the longer the time spent in annealing, and/or the slower the cooling rate before subsequent melting, the more stable the material will be for an increasing temperature range above the annealing temperature. By that, during heating, possibilities of recrystallisation are decreased or even prohibited in which latter case only melting is left.

Clearly, the phenomena seen also link up with temperature-modulated differential scanning calorimetry (TMDSC) experiments in which, depending on the thermal history, also excess phenomena are seen [16–18].

Conclusions

The measurements with the adiabatic calorimeter have resulted in very accurate heat capacity data for this ethylene-1-octene copolymer over a large temperature range. Using these data, the mass fraction crystallinity of this polymer was calculated: w^c=0.254 for temperatures below 230 K. In the temperature range from 230 to 360 K the crystallinity gradually decreases to zero because of melting.

The temperature drifts that are observed in the stabilisation periods clearly indicate relaxation processes around 215 K (devitrification at maximum), above annealing temperatures (only melting) and at temperatures in the melting region that must be interpreted as recrystallisation. These data may be quantified and can be of great importance for better interpreting TMDSC measurements in the melting region of polymers.

References

1 V. B. F. Mathot (Ed.), Calorimetry and Thermal Analysis of Polymers, Hanser Publishers, Munich, Vienna, New York 1994.
2 J. C. van Miltenburg, V. B. F. Mathot, P. J. van Ekeren and L. D. Ionescu, J. Therm. Anal. Cal., 56 (1999) 1017.
3 S. Hosoda, A. Uemura, Y. Shigematsu, I. Yamaamoto and K. Kojima, Stud. Surf. Sci. Catal., 89 (1994) 365.
4 Y.-C. Hwang, S. Chum, R. Guerra and K. Sehanobish, Antec '94 SPE Conf. Proc., Vol. III (1994) 3414.
5 J. C. van Miltenburg, A. C. G. van Genderen and G. J. K. van den Berg, Thermochim. Acta, 319 (1998) 151.

6 J. C. van Miltenburg, G. J. K. van den Berg and M. J. van Bommel, J. Chem. Thermodyn., 19 (1987) 1129.
7 H. Preston-Thomas, Metrologia, 27 (1990) 3 and Metrologia, 27 (1990) 107.
8 B. Wunderlich and G. Czornyj, Macromolecules, 10 (1977) 906.
9 V. B. F. Mathot, Polymer, 25 (1984) 579.
10 ATHAS data bank. For a recent description see: B. Wunderlich, Pure and Appl. Chem., 67 (1995) 1019. Detailed information may also be found on the internet: http://web.utk.edu/~athas
11 V. B. F. Mathot, R. L. Scherrenberg, M. F. J. Pijpers and W. Bras, J. Thermal Anal., 46 (1996) 681.
12 V. B. F. Mathot, R. L. Scherrenberg, M. F. J. Pijpers and Y.M.T. Engelen, Structure, Crystallisation and Morphology of Homogeneous Ethylene-Propylene, Ethylene-1-Butene and Ethylene-1-Octene Copolymers with High Comonomer Contents, in: S. Hosoda (Ed.), The New Trends In Polyolefin Science and Applications, Research Signpost, Trivandrum (India) (1996) 71.
13 V. B. F. Mathot, Chapter 5: Thermal Characterization of States of Matter, in: V. B. F. Mathot (Ed.), Calorimetry and Thermal Analysis of Polymers, Hanser Publishers, Munich, Vienna, New York 1994, p. 105.
14 P. J. van Ekeren, Chapter 2: Thermodynamic Background to Thermal Analysis and Calorimetry, in: M. E. Brown (Ed.), Handbook of Thermal Analysis and Calorimetry. Volume I: Principles and Practice, Elsevier, Amsterdam 1998, p. 75.
15 V. B. F. Mathot, R. L. Scherrenberg and M. F. J. Pijpers, Polymer, 39 (1998) 4541.
16 R. Scherrenberg, V. Mathot and A. van Hemelrijck, Thermochim. Acta, 330 (1999) 3.
17 R. Androsch, Polymer, 40 (1999) 2805.
18 A. Wurm, M. Merzlyakov and C. Schick, Thermochim. Acta, 330 (1999) 121.